

# Lab on a Chip

Accepted Manuscript



This is an *Accepted Manuscript*, which has been through the Royal Society of Chemistry peer review process and has been accepted for publication.

*Accepted Manuscripts* are published online shortly after acceptance, before technical editing, formatting and proof reading. Using this free service, authors can make their results available to the community, in citable form, before we publish the edited article. We will replace this *Accepted Manuscript* with the edited and formatted *Advance Article* as soon as it is available.

You can find more information about *Accepted Manuscripts* in the [Information for Authors](#).

Please note that technical editing may introduce minor changes to the text and/or graphics, which may alter content. The journal's standard [Terms & Conditions](#) and the [Ethical guidelines](#) still apply. In no event shall the Royal Society of Chemistry be held responsible for any errors or omissions in this *Accepted Manuscript* or any consequences arising from the use of any information it contains.

## Controllable Generation and Encapsulation of Alginate Fibers Using Droplet-Based Microfluidics

Chiara Martino<sup>\*</sup>, Cyril Statzer, Daniele Vigolo<sup>#</sup>, Andrew J. deMello<sup>\*</sup>

Department of Chemistry and Applied Biosciences, Institute for Chemical and Bioengineering, ETH Zurich, Vladimir Prelog Weg 1, Zürich 8093, Switzerland.

<sup>#</sup>Present address: School of Chemical Engineering, University of Birmingham, Edgbaston, Birmingham, B15 2TT, UK. <sup>\*</sup> E-mail: [andrew.demello@chem.ethz.ch](mailto:andrew.demello@chem.ethz.ch); [chiara.martino@chem.ethz.ch](mailto:chiara.martino@chem.ethz.ch)

**Herein we demonstrate the segmentation of alginate solution streams to generate alginate fibers of precisely controllable lengths between 200 and 1000  $\mu\text{m}$ . Moreover, we demonstrate the subsequent encapsulation of the formed fibers within pL-volume microdroplets, produced within the same microfluidic device, in a direct manner. Finally, we show immediate and complete on-chip gelation of alginate fibers in a rapid and reproducible fashion.**

### 1 Introduction

Over the last decade, the fabrication of fibrous structures on the micron scale has found numerous applications in the field of regenerative medicine<sup>1</sup> and tissue engineering<sup>2</sup>. In this regard, microfluidics has proved to be of great utility in generating chemically complex structures of tuneable geometry and in the handling of associated biomaterials<sup>3, 4</sup>. Amongst a great variety of naturally-derived materials used for hydrogel generation in biomedical applications<sup>5</sup> (such as hyaluronic acid, chondroitin sulfate, chitin, chitosan, gelatin and alginate) alginate-based materials have gained particular popularity for the generation of fibrous structures<sup>3</sup>. Alginate is a naturally derived polysaccharide, which is soluble in aqueous solutions and undergoes gelation when exposed to cations such as  $\text{Ca}^{2+}$ <sup>6</sup>. Once cross-linked, alginate forms a three-dimensional (3D) elastic network with high water content, representing a favourable substrate in which to mimic the extracellular matrix (ECM) in artificial cell systems<sup>7</sup>. Moreover, facile gelation, the ability of this material to hold live cells (such as fibroblasts<sup>8</sup>, myoblasts<sup>9</sup> and neuronal cells<sup>10</sup>) and its biocompatibility, are key properties that have been widely exploited in various fields including drug delivery<sup>11</sup>, food formulation<sup>12, 13</sup> and tissue engineering<sup>5, 14</sup>.

Microfluidic systems have proved particularly advantageous in allowing the fabrication of alginate hydrogels in a rich variety of geometries. Indeed, to date, alginate spheres<sup>15, 16</sup>, core-shell structures<sup>7, 17, 18</sup>, tear-drops<sup>19, 20</sup>, yarn-ball geometries<sup>21</sup>, full fibers<sup>22-24</sup>, hollow fibers<sup>25</sup> and patterned fibers<sup>10</sup> have all been successfully synthesized. However, it is noted that to date no method that allows the production and *in-situ* encapsulation of alginate fibers of defined length has been reported.

Alginate solutions exhibit viscoelastic shear-thinning behaviour, meaning that viscosity decreases with increasing strain rate<sup>26</sup>. On the molecular level, the long polymeric chains align when they are sheared and are able to slide along one another under high strain rate<sup>27</sup>, hence making alginate jet cutting inherently difficult. Herein, we present a strategy that allows: (i) the separation of a jet of alginate precursor solution prior to crosslinking, (ii) the immediate and complete gelation of alginate segments that prevents non-specific surface adhesion (which leads to fiber deformation and

ultimately channel blockage) and (iii) the encapsulation of alginate fibers within pL-volume droplets generated within the same microfluidic device (Figure 1).

By applying a pulsatile pressure regime to a sheathing buffer solution (defined as  $P_B$  in Figure 1), tuned to the alginate solution viscosity, we are able to periodically cut the alginate jet (controlled by  $P_A$ ). The alginate solution fragment travels into the polymerization channel where it first meets a buffer stream containing  $\text{Ca}^{2+}$  ions (Figure 1b-c) and subsequently an oil stream (controlled by  $P_O$  in Figure 1d) that is responsible for encapsulating the formed fibers into droplets. In contrast to prior studies that utilize a device-embedded valve for “cutting” polyethylene (glycol) diacrylate (400 Da) jets at pressures above 2 bar<sup>28</sup>, we are able to achieve cutting using pressures of only a few *mbars*, hence not affecting the downstream flows. Such an approach not only allows direct alginate segmentation but is also compatible with downstream droplet generation within the same microfluidic device. A detailed comparison between the presented approach and a lateral valve approach used for controlling polyethylene (glycol) diacrylate fiber lengths is presented in the Electronic Supplementary Information (ESI).

## 2 Experimental

### Materials

A 1% (w/w) sodium alginic acid salt solution was supplemented with fluorescent beads (F8809, FluoSpheres, carboxylate-modified orange 540/560, 0.2  $\mu\text{m}$ , Life Technologies, Switzerland). A 10% (w/w) dextran solution (31392 from *Leuconostoc* SPP,  $M_r$  450000 – 650000, Sigma-Aldrich, Switzerland) and a 10% (w/w) dextran solution supplemented with 100 mM CaCl (Sigma-Aldrich, Switzerland) were used as sheathing and polymerizing buffers respectively. Droplets were generated using a mineral oil continuous phase (M3516, Sigma-Aldrich, Switzerland) containing 2% (w/w) Span80 (S6770, Sigma-Aldrich, Switzerland).

All solutions were regulated using a pressure controller (OB1, Elveflow, France) in combination with proprietary software (Elveflow Smart Interface, Elveflow, France). The pressure ranges for the alginate precursor solution, sheathing buffer, calcium solution and oil were 80 – 130 mbar, 40 – 190 mbar, 100 – 170 mbar and 200 – 500 mbar respectively. The lateral valve (used in control experiments) was actuated with a customised solenoid valve system (MH1, Festo, Switzerland) with applied pressures ranging from 100 to 3000 mbar.

### Experimental setup

The microfluidic device design includes inlet channels for reagent delivery, a 1 cm long polymerization channel, a cross junction for droplet generation and a lateral valve (used for the control experiments described in the ESI). Devices were produced using standard soft lithographic methods<sup>29</sup> in polydimethylsiloxane (PDMS). The PDMS base and curing agent (Sylgard 184, Dow Corning, USA) were mixed at a ratio of 17:1 (w/w), degassed and decanted onto the master. The entire structure was cured in the oven at 70 °C overnight and then peeled off the master. After punching inlet and outlet vias, the structured PDMS layer was irreversibly bonded to a clean coverglass slide (76 mm x 26 mm x 1 mm, Menzel Gläser, USA) after exposing the two surfaces to an oxygen plasma (Dieter Electronics, USA) and cured on a hot plate at 120 °C for 1 hour. To limit unwanted alginate deposition on microchannel surfaces all devices were passivated with a 1% (w/w) solution of Pluronic F-127 (P2443, Sigma-Aldrich, Switzerland) in DPBS (14190, Life Technologies, Switzerland) for 1 hour and kept at 70 °C to dry.

All optical measurements were performed using an inverted microscope (Nikon Eclipse Ti-E, Nikon, Japan) equipped with a digital camera (Orca-Flash 4.0, Hamamatsu, Japan) and a light source (LED, Prior Scientific, United Kingdom) for bright field illumination. For fluorescence measurements a mercury light source (Intensilight C-HGFI, Nikon, Japan) in combination with a Tetramethylrhodamine (TRITC) filter set (F26-516, AHF analysentechnik AG, Germany) was utilized. Images were acquired using proprietary software (HCImageLive 4.0.3.6, Hamamatsu, Japan).

Fiber lengths were calculated from fluorescence signals recorded at the cross junction (Figure 1d), and fiber length quantification automatically processed using a script written in ImageJ 1.48v (NIH, USA). Additional details regarding analysis are provided in the ESI.

### 3 Results and Discussion

#### Synthesis of alginate fibers with different lengths

To control alginate fiber generation we explored various pulsing regimes that led to the production of fiber length ranging from few hundreds of microns to a few millimetres. The pressures associated with the calcium chloride solution ( $P_C$ ) and oil ( $P_O$ ) were kept constant across all the measurements (110 mbar and 350 mbar respectively), with  $P_C$  set at a value between  $P_{B\_low}$  and  $P_{B\_high}$ . Moreover, the alginate solution pressure ( $P_A$ ) was essentially kept constant but, according to the chosen  $\Delta P_B$  for each experiment,  $P_A$  was marginally adjusted to avoid alginate backflow.

Figure 2 illustrates representative data produced by two different pulsing regimes. In each regime, we applied an identical pulsation period and duty cycle (i.e. the fraction of time in which the pressure is kept high compared to the total period time) but different  $P_B$  pressure values ( $P_{B\_low}/P_{B\_high}$ ). As shown in Figure 2a-b,  $P_B$  followed a square wave signal with a period of 0.6 s and a 68% duty cycle, and  $P_B$  pressures were set at 90/140 mbar (Figure 2a) and 140/160 mbar (Figure 2b). It can be seen that variation of  $P_B$  led to a significant change in the fiber length, producing average fiber lengths of  $309 \pm 17 \mu\text{m}$  and  $717 \pm 72 \mu\text{m}$  (extracted from between 100 replicate measurements; Figure 2c).

We also investigated the combined effect of changing the pulsation period and  $P_B$  pressure values whilst maintaining a constant duty cycle of 68%. Figure 3a-c shows three different conditions that generate fibers of distinct lengths. In these experiments,  $P_B$  followed a square wave signal with a period of 0.4 s and values set to 70/130 mbar (Figure 3a and condition I in Figure 3d), a period of 0.9 s and values set to 120/160 mbar (Figure 3b, condition II in Figure 3d) and a period of 0.6 s and values set to 120/160 mbar (Figure 3c, condition III in Figure 3d). As shown in Figure 3d, such operating conditions generated fibers with lengths ranging from approximately 200 to 1000  $\mu\text{m}$ .

A more detailed summary of the variety of conditions analysed is presented in the ESI and demonstrates that an increase in  $P_{B\_low}$ , and a consequent increase of  $P_A$ , leads to a fiber length increase. Nevertheless, it is important to note that it is difficult to establish a strict relation between a single parameter and the alginate fiber length, since the experimental parameters are interdependent and cannot easily be changed in isolation. However, it is clear that the combination of a pulsatile sheathing buffer pressure and the spatial proximity of the sheathing buffer and calcium influx is essential to segment the alginate jet. Furthermore, the immediate calcium exposure favours fiber gelation over the re-joining of two consecutive un-polymerised alginate segments, with the backflow of  $\text{Ca}^{2+}$  ions in the buffer channel guaranteeing fast gelation of each alginate segment.

### Synthesis of patterned alginate fibers

As previously noted, a mild backflow of  $\text{Ca}^{2+}$  ions in the sheathing buffer channel accelerates alginate polymerization without causing alginate deposition. However, if  $P_A$  is increased and the lower buffer pressure ( $P_{B,low}$ ) decreased, the precursor alginate solution is able to flow into the sheathing buffer channel where it polymerizes leaving an imprint on the alginate fiber. Figure 4a-f shows a time sequence of a single cycle whilst Figure 4g shows an alginate fiber containing repetitive units obtained from channel imprinting after two cycles. Fibers were generated with  $P_A = 129$  mbar,  $P_B = 40/160$  mbar and a period and duty cycle equal to 0.6 s and 68% respectively.

### Fiber encapsulation

Alginate fibers generated by using  $P_A = 109$  mbar and  $P_B = 100/160$  mbar with period equal to 0.4 s, a 50% duty cycle and  $P_C = 110$  mbar could be directly encapsulated into pL-volume droplets.  $P_D$  was set to 350 mbar and droplets of an average diameter of 186  $\mu\text{m}$  (C.V.= 5%) were produced at a frequency of 8.4 Hz. Figure 5a-d shows representative time frames during the encapsulation of a 300  $\mu\text{m}$  long alginate fiber. Under the current operating conditions one out of three droplets could be loaded with an *in situ* generated fiber. As shown in Figure 5e, the fiber encapsulation process does not affect droplet diameter. Moreover, small variations in oil pressure ( $\pm 10\%$ ) did not affect upstream fiber generation, thus allowing control over both droplet size and fiber encapsulation. To ascertain whether gelation of the alginate fiber occurred within the device, a drop (100  $\mu\text{L}$ ) of the emulsion produced on-chip was deposited and smeared onto a coverglass slide (Figure 5f). No significant deformation in fiber shape could be observed and imaging of droplets containing alginate fibers 1 hour after generation confirmed that alginate fiber shape was identical to that observed during encapsulation (Figure 5g).

### Fouling

Fouling is a common problem encountered in microfluidic devices, especially when directly bonded on glass surfaces since glass has a very high nonspecific binding capacity for proteins and other biomolecules<sup>30</sup>. A number of methods have been developed to limit this problem<sup>31</sup>. In this work, surface treatment with Pluronic-127 was successful in preventing fouling when compared to uncoated devices. The time until the first alginate deposition occurred increased from approximately 1 minute, in uncoated devices, to between 5 and 10 minutes when coated with Pluronic-127. Furthermore, fouling on the coated surface displayed a much weaker attachment and, thus could be removed immediately by the next fiber. We also observed that this “self-cleaning” effect was more efficient when the diameter of the polymerization channel was smaller, since the fiber was less likely to pass around the attached fibers. If such a self-cleaning process proved ineffective, an increase in alginate pressure for two seconds was used to purge the polymerization channel, giving the devices a working lifetime of up to 60 minutes.

## 4 Conclusions

In this work, we present a new microfluidic strategy to segment an alginate precursor solution and generate alginate fibers. The combined effects of pulsatile pressure control and immediate exposure to a buffer solution containing  $\text{Ca}^{2+}$  ions are responsible for the generation of alginate fibers of different lengths, ranging from a few hundreds of microns to up to one millimetre. Alginate fibers of different length are of potential utility in culturing small cell populations in spatially defined environments and in a high-throughput manner, thus enabling hydrogel-shape dependent studies of

cellular behaviour (as well as unlocking potential applications in biofabrication). Our approach is highly successful in achieving fast alginate gelation over very short distances, which in turn allows the encapsulation of polymerised fibers within the same microfluidic device. This feature will be particularly interesting in droplet-based application, for example for the generation of artificial cell constructs<sup>32, 33</sup> containing inner scaffolding. In this way it is possible to generate systems that can mimic functions of cells like the presence of a membrane setting a boundary of an inner compartment of controlled and well defined geometry. We can predict that the construction of such entities not only will offer the possibility of replacing faulty biological components in individuals affected by severe pathologies, as it is already happening for microfabricated tissue engineering products<sup>3</sup>, but will also facilitate the understanding of components of life by making from scratch.

### Acknowledgements

CM acknowledges support from the ETH Zurich Postdoctoral Fellowship Program and Marie Curie Actions for People COFUND Program.

### References

1. H. Onoe and S. Takeuchi, *Drug Discovery Today*, 2015, **20**, 236-246.
2. A. Tamayol, M. Akbari, N. Annabi, A. Paul, A. Khademhosseini and D. Juncker, *Biotechnology Advances*, 2013, **31**, 669-687.
3. M. A. Daniele, D. A. Boyd, A. A. Adams and F. S. Ligler, *Advanced Healthcare Materials*, 2015, **4**, 2-2.
4. K. Ren, Y. Chen and H. Wu, *Current Opinion in Biotechnology*, 2014, **25**, 78-85.
5. B. G. Chung, K.-H. Lee, A. Khademhosseini and S.-H. Lee, *Lab on a Chip*, 2012, **12**, 45-59.
6. I. Machida-Sano, M. Hirakawa, H. Matsumoto, M. Kamada, S. Ogawa, N. Satoh and H. Namiki, *Biomedical materials*, 2014, **9**, 025007.
7. C. Martino, T. Y. Lee, S.-H. Kim and A. J. deMello, *Biomicrofluidics*, 2015, **9**, 024101.
8. K. Y. Lee, E. Alsberg, S. Hsiang, W. Comisar, J. Linderman, R. Ziff and D. Mooney, *Nano Letters*, 2004, **4**, 1501-1506.
9. E. Alsberg, K. W. Anderson, A. Albeiruti, R. T. Franceschi and D. J. Mooney, *Journal of dental research*, 2001, **80**, 2025-2029.
10. Y. Kitagawa, Y. Naganuma, Y. Yajima, M. Yamada and M. Seki, *Biofabrication*, 2014, **6**, 035011.
11. T. W. Wong, *Journal of Pharmacy and Pharmacology*, 2011, **63**, 1497-1512.
12. L. H. Pignolet, A. S. Waldman, L. Schechinger, G. Govindarajoo, J. S. Nowick and L. Ted, *Journal of Chemical Education*, 1998, **75**, 1430.
13. A. Escarpa, *Lab on a Chip*, 2014, **14**, 3213-3224.
14. K. Y. Lee and D. J. Mooney, *Progress in Polymer Science*, 2012, **37**, 106-126.
15. S. Sugaya, M. Yamada, A. Hori and M. Seki, *Biomicrofluidics*, 2013, **7**, 054120.
16. W. H. Tan and S. Takeuchi, *Advanced Materials*, 2007, **19**, 2696-2701.
17. P.-W. Ren, X.-J. Ju, R. Xie and L.-Y. Chu, *Journal of Colloid and Interface Science*, 2010, **343**, 392-395.
18. J. Wu, T. Kong, K. W. K. Yeung, H. C. Shum, K. M. C. Cheung, L. Wang and M. K. T. To, *Acta biomaterialia*, 2013, **9**, 7410-7419.

19. C. J. Martinez, J. W. Kim, C. Ye, I. Ortiz, A. C. Rowat, M. Marquez and D. Weitz, *Macromolecular Bioscience*, 2012, **12**, 946-951.
20. Y. Hu, G. Azadi and A. M. Ardekani, *Carbohydrate Polymers*, 2015, **120**, 38-45.
21. A. Miyama, M. Yamada, S. Sugaya and M. Seki, *RSC Advances*, 2013, **3**, 12299-12306.
22. M. Yamada, S. Sugaya, Y. Naganuma and M. Seki, *Soft Matter*, 2012, **8**, 3122-3130.
23. E. Kang, S.-J. Shin, K. H. Lee and S.-H. Lee, *Lab on a Chip*, 2010, **10**, 1856-1861.
24. S.-J. Shin, J.-Y. Park, J.-Y. Lee, H. Park, Y.-D. Park, K.-B. Lee, C.-M. Whang and S.-H. Lee, *Langmuir*, 2007, **23**, 9104-9108.
25. K. H. Lee, S. J. Shin, Y. Park and S.-H. Lee, *Small*, 2009, **5**, 1264-1268.
26. R. A. Rezende, P. J. Bártolo, A. Mendes and R. M. Filho, *Journal of Applied Polymer Science*, 2009, **113**, 3866-3871.
27. K. Brian, *Micro- and Nanoscale Fluid Mechanics Transport in Microfluidic Devices*, Cambridge University Press, 2009.
28. J. K. Nunes, K. Sadlej, J. I. Tam and H. A. Stone, *Lab on a Chip*, 2012, **12**, 2301-2304.
29. Y. N. Xia and G. M. Whitesides, *Angew Chem Int Edit*, 1998, **37**, 550-575.
30. P. K. Sorger, *Nat Biotech*, 2008, **26**, 1345-1346.
31. I. Banerjee, R. C. Pangule and R. S. Kane, *Advanced Materials*, 2011, **23**, 690-718.
32. C. Martino, L. Horsfall, Y. Chen, M. Chanasakulniyom, D. Paterson, A. Brunet, S. Rosser, Y.-J. Yuan and J. M. Cooper, *ChemBioChem*, 2012, **13**, 792-795.
33. C. Martino, S.-H. Kim, L. Horsfall, A. Abbaspourrad, S. J. Rosser, J. Cooper and D. A. Weitz, *Angewandte Chemie International Edition*, 2012, **51**, 6416-6420.



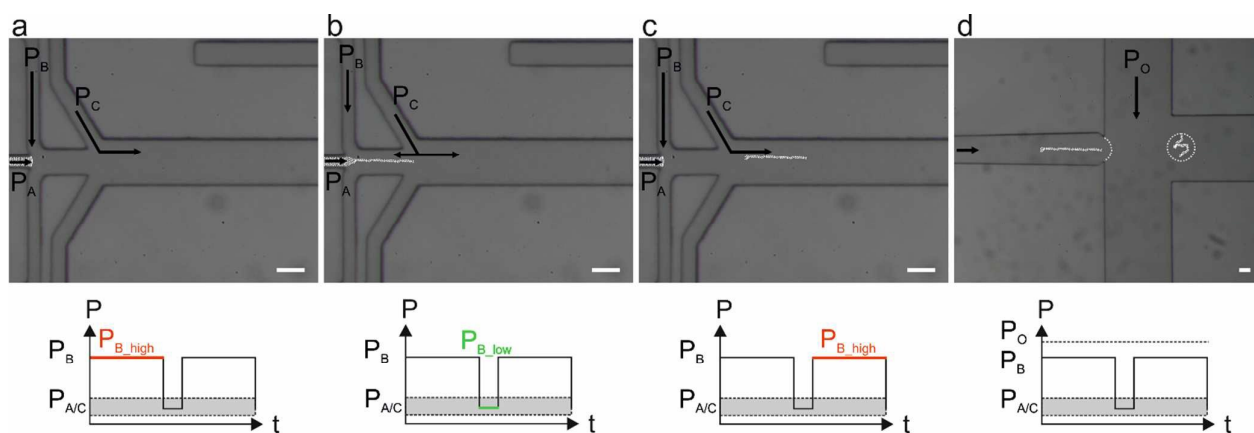


**Figure 1 Working principle for the generation and encapsulation of alginate fibers.** (a-c) Optical images of the microfluidic device containing multiple inlet channels and an indication of the pressures adopted to segment an alginate input stream. Pressures of an aqueous alginate precursor solution (A), a sheathing buffer solution (B) and a buffer solution containing  $\text{Ca}^{2+}$  ions (C) are set by a pressure controller.  $P_A$  and  $P_C$  are kept constant whereas  $P_B$  follows a square wave function. Under these conditions an imposed variation in  $P_B$  ( $\Delta P_B$ ) causes a discontinuous flow of A and a slight backflow of C. The gelation of A occurs due to  $\text{Ca}^{2+}$  ion diffusion from the side flows and to the convective movement caused by backflow of C. (d) Optical image of the microfluidic device at the cross junction where the aqueous solutions meet an oil phase (O). The cross junction is designed to be 1 cm away from the alginate channel to ensure complete alginate polymerization prior to encapsulation. Scale bars are equal to  $50 \mu\text{m}$ .



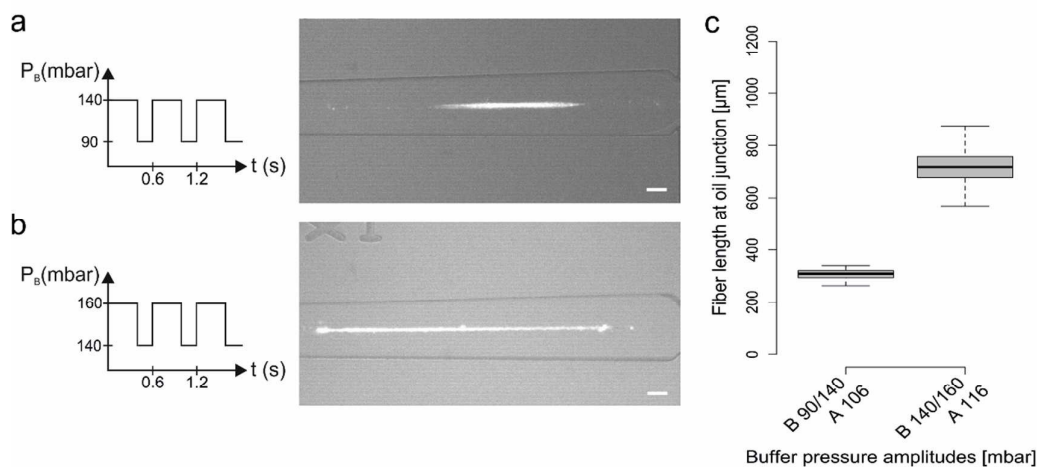


**Figure 2 Generation of alginate fibers using a constant  $P_B$  pulsation period and different  $P_B$  pressure values.** (a-b) Two operating conditions, which differ in  $P_{B\_low}/P_{B\_high}$  values and alginate pressure, produce different fiber lengths at the end of the polymerization channel. In both experiments the duty cycle and pulsation period are equal to 68% and 0.6 s respectively. (c) Box plot of fiber lengths obtained at  $P_B = 90/140$  mbar,  $P_A = 106$  mbar and  $P_B = 140/160$  mbar,  $P_A = 116$  mbar showing two distinct fiber populations with average lengths equal to  $309 \pm 17 \mu\text{m}$  and  $717 \pm 72 \mu\text{m}$  respectively. Scale bars are equal to  $50 \mu\text{m}$ .

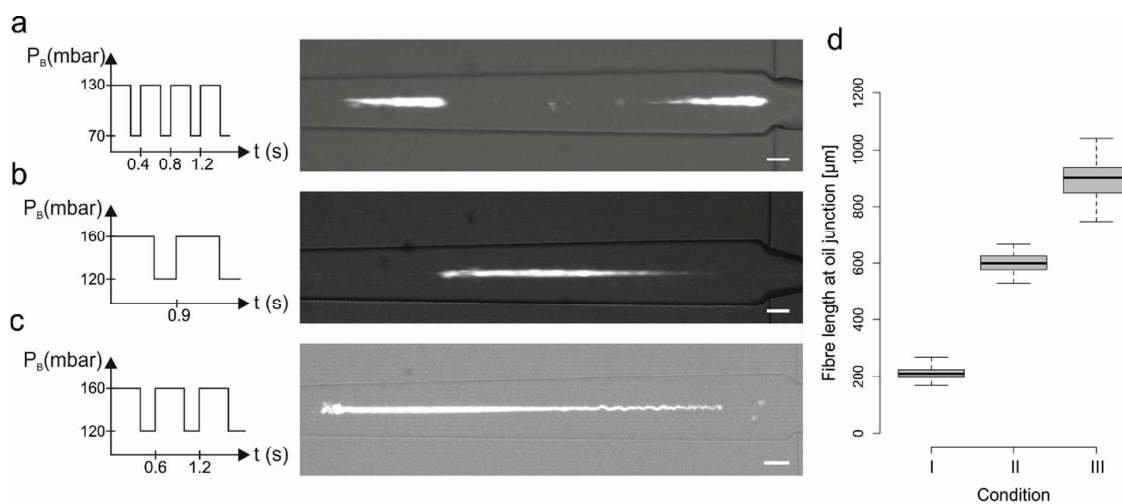


**Figure 3 Generation of alginate fibers using different  $P_B$  pulsation periods and different  $P_B$  pressures.** (a-c) Three operating conditions, which differ in pulsation period,  $P_{B\_low}/P_{B\_high}$  and alginate pressures, produce different fiber lengths at the end of the polymerization channel. For all conditions the duty cycle is equal to 68%. (d) Box plot of fiber lengths at three different conditions shows alginate fiber lengths of  $218 \pm 21 \mu\text{m}$  (condition I),  $598 \pm 33 \mu\text{m}$  (condition II) and  $900 \pm 106 \mu\text{m}$  (condition III). Condition I:  $P_A = 102 \text{ mbar}$  and  $P_B = 70/130 \text{ mbar}$  with a period equal to 0.4 s. Condition II:  $P_A = 115 \text{ mbar}$  and  $P_B = 120/160 \text{ mbar}$  with a period equal to 0.9 s. Condition III:  $P_A = 115 \text{ mbar}$  and  $P_B = 120/160 \text{ mbar}$  with a period of 0.6 s. Scale bars are equal to 50  $\mu\text{m}$ .

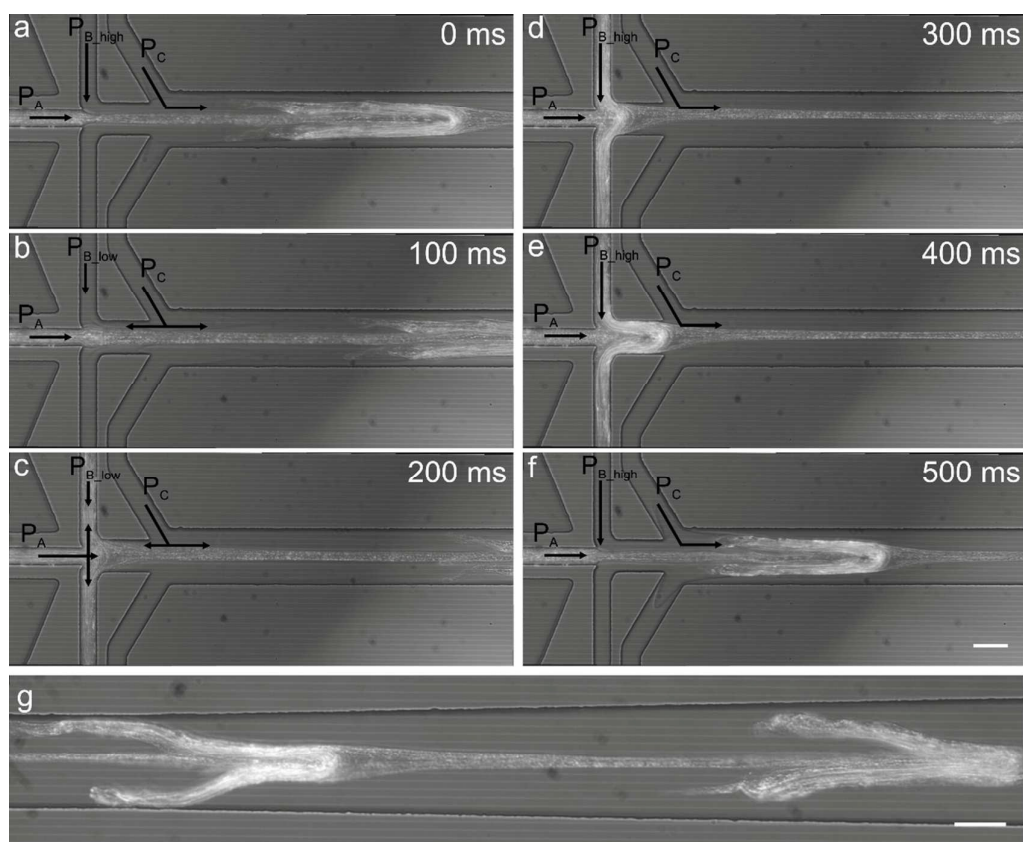


**Figure 4 Generation of regularly patterned alginate fibers.** A variation of the operating conditions imposed in Figure 2b leads to the production of a continuous alginate fiber displaying regular dispersed protrusions. This is achieved by increasing  $\Delta P_B$  and increasing the alginate pressure. Starting from the pressure conditions in Figure 2b, by decreasing the  $P_{B\_low}$  to 40 mbar and increasing the alginate pressure to 129 mbar the alginate solution and  $Ca^{2+}$  ions flow into the sheathing buffer channel and initiate gelation (a-c); as soon as the  $P_B$  becomes higher, the polymerised alginate is pushed out forming a fiber containing imprinted features (d-f) which flows downstream (g). Scale bars are equal to 50  $\mu m$ .

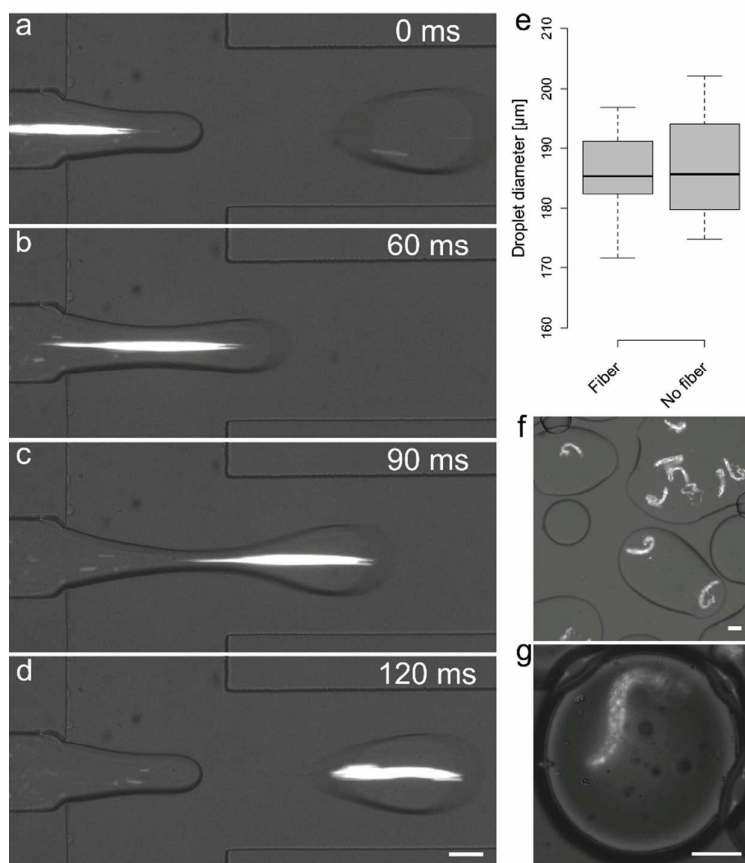


**Figure 5 Fiber encapsulation.** (a-d) Encapsulation of a single alginate fiber into a microdroplet occurring at the end of the polymerizing channel. Fibers were produced by setting  $P_A = 109$  mbar,  $P_B = 100/160$  mbar with period equal to 0.4 s and 50% duty cycle and  $P_C = 110$  mbar. (e) Box plot showing the diameters of filled ( $186 \pm 7$   $\mu\text{m}$ ) and empty droplets ( $187 \pm 8$   $\mu\text{m}$ ) generated using  $P_O = 350$  mbar. (f) Droplets collected outside the device and smeared on a coverglass slide, showing no change in fiber shape. (g) A representative droplet-encapsulated alginate fiber collected off chip 1 hour after generation, illustrating complete gelation and no significant shape change. Scale bars are equal to 50  $\mu\text{m}$ .